# Modeling of a Ring Rosen-Type Piezoelectric Transformer by Hamilton's Principle

Clément Nadal, François Pigache, Jiri Erhart

# Modeling of a Ring Rosen-Type Piezoelectric Transformer by Hamilton's Principle

Clément Nadal, François Pigache, and Jiří Erhart

***Abstract*—This paper deals with the analytical modeling of a ring Rosen-type piezoelectric transformer. The developed model is based on a Hamiltonian approach, enabling to obtain main parameters and performance evaluation for the first radial vibratory modes. Methodology is detailed, and final results, both the input admittance and the electric potential distribution on the surface of the secondary part, are compared with numerical and experimental ones for discussion and validation.**

## I. Introduction

The emergence of piezoelectric transformers (PTs) coincides with the development of ferroelectric ceramics belonging to the perovskite crystalline family in the 1950s. PTs use converse piezoelectric effect in the primary circuit and direct effect in the secondary circuit for ac voltage transformation. The first patent for a step-up PT was issued to Rosen *et al.* in 1958 in the well-known device today called a Rosen-type transformer [1]. In addition to providing small size and weight, PTs offer outstanding performance in terms of galvanic insulation, voltage ratio, and efficiency. Due to their obvious characteristics, since the 1990s, PTs have been widely used for low-power applications and small embedded systems such as ac/dc converters dedicated to laptop chargers [2] or electronic ballast for fluorescent lamps [3].

Recently, an outstanding interest has been demonstrated in the plasma generation field. It is true that the use of piezoelectric material for spark ignition has been known for a long time as attested by various patents about gas igniters [4], [5], but it has only been for about 15 years that this material is newly observed as an interesting plasma generator. This recent interest is obviously boosted by the widespread applications involving cold plasma discharges such as in biological field, dental surgery, and many others. The main special features of the PT solution are the high-voltage gain capability and the inherent high dielectric permittivity of the ferroelectric material. Several studies have been carried out with common rectangular Rosen-type transformers used as a cold plasma generator in different gases for several configurations [6], [7]. Moreover, specific high-voltage transformers have been designed with a view to plasma generation [8], [9], leading to patented designs [10].

Rosen *et al.* suggested not only rectangular geometry ($k_{31}$ – $k_{33}$ mode), but also variants for the disc ($k_{\mathrm{p}}$ – $k_{33}$ ) mode), ring ($k_{31}$ – $k_{33}$ mode), and tube ($k_{33}$ – $k_{33}$ mode) geometries. Detailed modeling of parameters for the rectangular Rosen-type transformers could be found (e.g., in [11], [12]) and for its thickness-shear modification in [13]. Circular geometry of the Rosen-type transformer has not been studied up to now in detail. An attempt has been made to model the ring-dot transformer (homogeneously poled) [14], or the ring-dot Rosen-type transformer equivalent circuit (poled in thickness direction for the primary part and in the radial direction for the secondary part) [15], or the tube transformer (poled radially in both segments) [16].

The main aim of the presented work is the development of an analytical method based on a Hamiltonian approach to study the electromechanical behavior of a ring Rosen-type PT. A first interesting study was proposed by Lin *et al.* [15] in which an electrical equivalent circuit of PT's vibratory behavior is obtained. From the latter, a parametric study was carried out on the geometric dependence of the resonance and anti-resonance frequencies. In this paper, a different approach is addressed. The idea of this article is to formulate the general equations of motion with an energetic method. A study of the PT's electric behavior will follow especially in terms of input admittance. The electric potential distribution will be also a major point of interest in view of the possible design of a cold plasma generator.

Finally, this article contains the following parts: the first one will be dedicated to the development of the electromechanical modeling whose equations are obtained from a Hamiltonian approach [12] and solved with the standard modal expansion method. The final model will be experimentally verified on prepared samples of ring Rosen-type transformer and also validated with numerical modeling based on the finite element method. The topic of the second section will be followed by a discussion on the relevance of the developed theoretical approach.

## II. Analytical Modeling

### A. Structure and Assumptions

*1) Geometry:* The analytical modeling developed below relies on a geometry of a ring Rosen-type PT as illustrated

Manuscript received October 9, 2014; accepted January 23, 2015.

C. Nadal is with the Laboratory of Electrical Engineering and Power Electronics (L2EP), Control Team, University of Lille 1, Villeneuve d'Ascq, Nord 59658, France (e-mail: Clement.Nadal@ircica.univ-lille1.fr).

F. Pigache is with the Laboratory on Plasma and Conversion of Energy, Electrodynamics Research Group, Institut National Polytechnique de Toulouse, FR-31071 Toulouse, France.

J. Erhart is with Technical University of Liberec, Piezoelectricity Research Laboratory, Liberec, Czech Republic, CZ-46117.

DOI http://dx.doi.org/10.1109/TUFFC.2014.006719

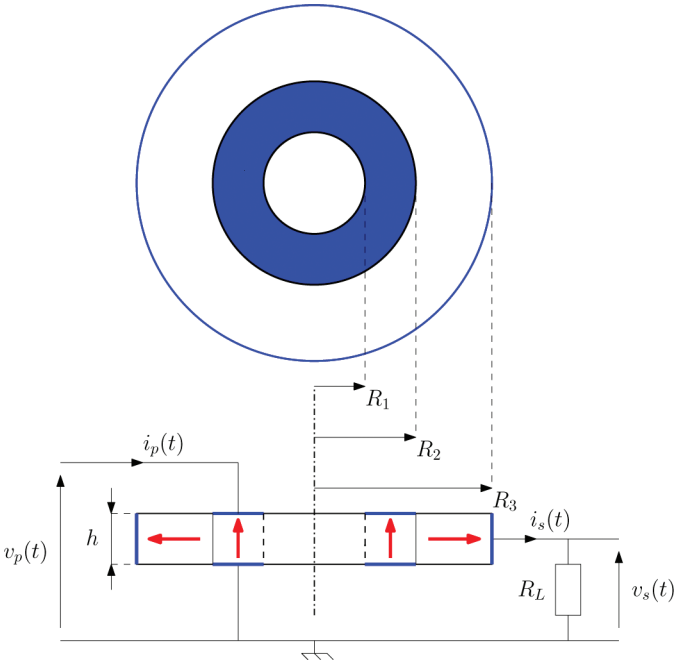

Fig. 1. Structure of a ring Rosen-type piezoelectric transformer.

in Fig. 1. The PT is composed of a primary part of inner radius $R_1$ and outer radius $R_2$ poled in the thickness direction and a secondary part radially polarized spreading from the radii $R_2$ to $R_3$. This architecture of thickness $h$ is driven by an ac voltage power supply applied to the driving section by means of two annular electrodes. At the receiving section, the electric charges generated by the direct piezoelectric effect are gathered on a cylindrical electrode with radius $R_3$ and height $h$ on the outer edge of the ring. Thereafter, the cylindrical coordinate system is chosen and its origin is put at the center of the transformer.

*2) Mechanical Hypothesis:* M1: Because the optimum performance of this structure is achieved for radial modes, the PT is considered as a thin hollow cylinder whose first radial modes are taken into account. This assumption needs to respect ($h \ll R_3$).

M2: A purely radial displacement assumption requires that the orthoradial displacement is negligible. Furthermore, the radial component of the displacement is supposed to be independent of the $\theta-$ and $z-$ coordinates due to the axisymmetry and low thickness. As a consequence, the following relationships are supposed to be verified:

$$u_\theta = 0 \text{ and } u_r(r,\theta,z,t) = u_r(r,t). \tag{1}$$

M3: The assumption of a plane stress motion is put forward. The normal stress, $T_{zz}$, and the shear stresses, $T_{\tau z}$ and $T_{\theta z}$, are consequently assumed to be zero. The last shear stress $T_{\tau\theta}$ is vanished due to the axisymmetry in such a way that

$$T_{zz} = T_{\theta z} = T_{rz} = T_{r\theta} = 0. \tag{2}$$

M4: The PT is supposed to be traction-free on its inner and outer edges, leading to the following conditions:

$$T_{rr}(r = R_1, t) = 0 \text{ and } T_{rr}(r = R_3, t) = 0. \tag{3}$$

*3) Electrical Hypothesis:* E1: The primary part being assumed reasonably thin and supplied from its lower and upper faces, the electric field $\mathbf{E}$, deriving from the electric potential $\phi$, is supposed to be only orientated along the $z$-axis leading to:

$$\mathbf{E} = [0 \quad 0 \quad -\phi_{,z}]^{\mathrm{T}}, \tag{4}$$

where $(.)_{,z}$ denotes a partial derivative with respect to the variable $z$ and a superscripted T indicates matrix transposition.

E2: The primary side is supposed to be respectively connected to the potential $v_{\mathrm{p}}(t)$ and the ground on its lower and upper faces so much that

$$\forall r \in [R_1, R_2], \begin{cases} \phi(r, z = h/2, t) = v_{\mathrm{p}}(t) \\ \phi(r, z = -h/2, t) = 0. \end{cases} \tag{5}$$

E3: As the secondary part is radially polarized, and besides, it is not electroded on its lower and upper faces, it is supposed that the electric displacement field $\mathbf{D}$ is purely radial as follows:

$$\mathbf{D} = [D_r \quad 0 \quad 0]^{\mathrm{T}}. \tag{6}$$

E4: The secondary part is supposed to be connected to a load resistance $R_{\mathrm{L}}$ so much that

$$\forall z \in [-h/2, h/2], \phi(r = R_3, z, t) = v_{\mathrm{s}}(t) = R_{\mathrm{L}} i_{\mathrm{s}}(t), \tag{7}$$

where $v_{\mathrm{s}}$ and $i_{\mathrm{s}}$ are the voltage at the terminals of the load resistance and the current through it, respectively.

### *B. Constitutive Relationships*

*1) Driving Section:* As the primary part behaves like an actuator, the set of two independent variables ($\mathbf{S}$, $\mathbf{E}$) is consequently chosen. These general constitutive relationships are reminded in [17, ch. 2, sec. 8, p. 51, eq. 2.8–5] where the material matrices are expressed in accordance with the axial polarization of the primary section. The application of the hypothesis M2, M3, and E1 on these constitutive relationships leads to

$$\begin{aligned} T_{rr} &= \bar{c}_{11}^E u_{r,r} + \bar{c}_{12}^E u_r/r - \bar{e}_{31} E_z \\ T_{\theta\theta} &= \bar{c}_{12}^E u_{r,r} + \bar{c}_{11}^E u_r/r - \bar{e}_{31} E_z \\ D_z &= \bar{e}_{31} u_{r,r} + \bar{e}_{31} u_r/r + \bar{\varepsilon}_{33}^S E_z, \end{aligned} \tag{8}$$

where the strain-displacement relationships $S_{rr} = u_{r,r}$ and $S_{\theta\theta} = u_r/r$ have been used. The bar symbol on the material coefficients is a note to use the specific value of the radial transverse coupling mode. These coefficients are

TABLE I. Piezoelectric Material Coefficients of the Radial Transverse Coupling Mode.

| | | |
|---|---|---|
| $\overline{c}_{11}^{E} = \frac{1}{s_{11}^{E}[1-(\sigma_{12}^{E})^2]}$ | $\overline{e}_{31} = \frac{d_{31}}{s_{11}^{E}(1-\sigma_{12}^{E})}$ | $\sigma_{12}^{E} = -\frac{s_{12}^{E}}{s_{11}^{E}}$ |
| $\overline{c}_{12}^{E} = \frac{\sigma_{12}^{E}}{s_{11}^{E}\left[1-(\sigma_{12}^{E})^2\right]}$ | $\overline{\varepsilon}_{33}^{S} = \varepsilon_{33}^{T}(1-k_{\mathrm{p}}^2)$ | $k_{\mathrm{p}} = k_{31}\sqrt{\frac{2}{1-\sigma_{12}^{E}}}$ |

given in Table I, where $\sigma_{12}^{E}$ and $k_{\mathrm{p}}$ are the Poisson's ratio at constant electric field and the material coupling factor relative to the radial transverse mode, respectively.

*2) Receiving Section:* As the secondary part behaves like a sensor, the set of two independent variables ($\mathbf{S}$, $\mathbf{D}$) is consequently chosen. As reminded in [17, ch. 2, sec. 8, p. 51, eq. 2.8–10] and according to M2, M3, and E2, the constitutive relationships are reduced to the following expression:

$$\begin{aligned} T_{rr} &= \overline{c}_{33}^{D}u_{r,r}+\overline{c}_{13}^{D}u_r/r - \overline{h}_{33}D_r \\ T_{\theta\theta} &= \overline{c}_{13}^{D}u_{r,r}+ \overline{c}_{11}^{D}u_r/r - \overline{h}_{31}D_r \\ \phi_{,r} &= \overline{h}_{33}u_{r,r} + \overline{h}_{31}u_r/r - \overline{\beta}_{33}^{S}D_r. \end{aligned} \tag{9}$$

The bar symbol on the material coefficients is a note to use the specific value of the radial longitudinal coupling mode. These coefficients are given in Table II, where $\sigma_{13}^{E}$ is the Poisson's ratio at constant electric field relative to the radial longitudinal mode.

### C. Determination of Electrical Quantities

*1) Electric Field in the Primary Part:* For the driving section, the electric displacement field is given by the following relationship:

$$D_z = \overline{e}_{31}u_{r,r} + \overline{e}_{31}u_r/r - \overline{\varepsilon}_{33}^{S}\phi_{,z}. \tag{10}$$

In fact, it results from the Gauss's law verified throughout piezoelectric material:

$$D_{z,z} = 0 \Leftrightarrow \phi_{,zz} = 0 \Leftrightarrow \phi(z,t) = A_{\phi}(t)z + B_{\phi}(t), \tag{11}$$

where $A_{\phi}$ and $B_{\phi}$ are two constants of integration function of the time $t$. They can be determined from E2 so much that the electric potential in the driving section is expressed as follows:

$$\phi(z,t) = \frac{v_{\mathrm{p}}(t)}{h}\Big(z+\frac{h}{2}\Big), \tag{12}$$

and the $z$-axis component of the electric field is

$$E_z(t) = -\frac{v_{\mathrm{p}}(t)}{h}. \tag{13}$$

*2) Electric Displacement Field in the Secondary Part:* For the receiving section, the electric displacement field is given from the Gauss's law verified throughout piezoelectric material by

$$D_{r,r} + \frac{1}{r}D_r = 0 \Leftrightarrow D_r(r,t) = \frac{C_{\phi}(t)}{\overline{\beta}_{33}^{S}r}, \tag{14}$$

where $C_{\phi}$ is a constant of integration function of the time $t$. The latter can be determined from the quantity of electric charges $q_{\mathrm{s}}$ gathered on the edge of the secondary section defined as follows:

$$q_{\mathrm{s}}(t) = -\int_0^{2\pi}\int_{-(h/2)}^{h/2} D_r(r=R_3,t)R_3\mathrm{d}\theta\mathrm{d}z, \tag{15}$$

so much that

$$D_r(r,t) = -\frac{q_{\mathrm{s}}(t)}{2\pi r h}. \tag{16}$$

### D. Lagrangian of the Piezoelectric Transformer

The Lagrangian $\mathcal{L}$ of the studied system is the sum of two contributions corresponding to the primary and secondary parts so much that

$$\mathcal{L} = \mathcal{L}_{\mathrm{p}} + \mathcal{L}_{\mathrm{s}}. \tag{17}$$

Each term of the previous relationship is classically defined by the difference of a kinetic coenergy $\mathcal{T}^*$ and a po-

TABLE II. Piezoelectric Material Coefficients of the Radial Longitudinal Coupling Mode.

| | | |
|---|---|---|
| $\overline{c}_{11}^{D} = \frac{1-k_{33}^2}{s_{11}^{E}\delta}$ | $\overline{h}_{31} = \frac{k_{31}(k_{31}+k_{33}\sigma_{13}^{E})}{d_{31}\delta}$ | $\overline{\beta}_{33}^{S} = \frac{1-(\sigma_{13}^{E})^2}{\varepsilon_{33}^{T}\delta}$ |
| $\overline{c}_{13}^{D} = \frac{k_{31}k_{33}+\sigma_{13}^{E}}{\delta\sqrt{s_{11}^{E}s_{33}^{E}}}$ | $\overline{h}_{33} = \frac{k_{33}(k_{33}+k_{31}\sigma_{13}^{E})}{d_{33}\delta}$ | $\sigma_{13}^{E} = -\frac{s_{13}^{E}}{\sqrt{s_{11}^{E}s_{33}^{E}}}$ |
| $\overline{c}_{33}^{D} = \frac{1-k_{31}^2}{s_{33}^{E}\delta}$ | $\delta = (1-k_{31}^2)(1-k_{33}^2) - (k_{31}k_{33}+\sigma_{13}^{E})^2$ | |

tential energy $\mathcal{U}$. If there is no ambiguity on the definition of $\mathcal{U}$ in a purely mechanical framework, it differs for a piezoelectric system in accordance with the function, actuator or sensor, accomplished by this one. It can be summed up in the following way:

- Primary part = actuator: To study such a behavior, the independent variable set ($\mathbf{S}$, $\mathbf{E}$) has been chosen (see Section II-B). The potential energy $\mathcal{U}$ thus identifies with a free enthalpy $\mathcal{G}_2^a$ so much that the Lagrangian of the primary part is written as follows [18, ch. 2, sec. 2.5.2, p. 16, Table 2.1]:

$$\mathcal{L}_{\mathrm{p}} = \frac{1}{2}\int_{\Omega_{\mathrm{p}}} [\rho_{\mathrm{p}}\dot{\mathbf{u}}^{\mathrm{T}}\dot{\mathbf{u}} - \mathbf{S}^{\mathrm{T}}[c^{E}]\mathbf{S} + 2\mathbf{S}^{\mathrm{T}}[e]^{\mathrm{T}}\mathbf{E} + \mathbf{E}^{\mathrm{T}}[\varepsilon^{S}]\mathbf{E}]\mathrm{d}\Omega, \tag{18}$$

  where $\rho_{\mathrm{p}}$ and $\Omega_{\mathrm{p}}$ are, respectively, the mass density and the volume of the primary section. This convention goes hand in hand with a displacement/flux linkage formulation based on the use of the generalized coordinates and velocities ($\mathbf{u}$, $\lambda_{\mathrm{p}}$) and ($\dot{\mathbf{u}}, v_{\mathrm{p}}$), respectively. The expression (18) can be made explicit by using the strain-displacement relationships and the electric field $E_z$ in the driving section given by (13) leading to expression (22). The clamped capacitance of the driving section has been defined with the following expression:

$$C_{\mathrm{p}} = \overline{\varepsilon}_{33}^{S}\frac{\pi(R_2^2 - R_1^2)}{h}. \tag{19}$$

- Secondary part = sensor: For this function accomplished by the secondary section, the independent variable set ($\mathbf{S}$, $\mathbf{D}$) has been chosen (see Section II-B). The potential energy $\mathcal{U}$ thus identifies with a free energy $\mathcal{F}^s$ so much that the Lagrangian of the secondary part is written as follows [18, ch. 2, sec. 2.5.2, p. 16, Table 2.1]:

$$\mathcal{L}_{\mathrm{s}} = \frac{1}{2}\int_{\Omega_{\mathrm{s}}} [\rho_{\mathrm{s}}\dot{\mathbf{u}}^{\mathrm{T}}\dot{\mathbf{u}} - \mathbf{S}^{\mathrm{T}}[c^{D}]\mathbf{S} + 2\mathbf{S}^{\mathrm{T}}[h]^{\mathrm{T}}\mathbf{D} - \mathbf{D}^{\mathrm{T}}[\beta^{S}]\mathbf{D}]\mathrm{d}\Omega, \tag{20}$$

  where $\rho_{\mathrm{s}}$ and $\Omega_{\mathrm{s}}$ are the mass density and the volume of the receiving part, respectively. This convention goes hand in hand with a displacement/charge formulation based on the use of the generalized coordinates and velocities ($\mathbf{u}$, $q_{\mathrm{s}}$) and ($\dot{\mathbf{u}}, i_{\mathrm{s}}$), respectively. The expression (20) can be made explicit by using the strain-displacement relationships and the electric displacement field $D_r$ in the receiving section given by (16) leading to the expression (23) with $\nu = (\overline{c}_{11}^{D}/\overline{c}_{33}^{D})^{1/2}$ and $\overline{\sigma}_{13}^{D} = \overline{c}_{13}^{D}/\overline{c}_{33}^{D}$. The clamped capacitance of the receiving section has been introduced by means of the following relationship:

$$C_{\mathrm{s}} = \frac{2\pi h}{\overline{\beta}_{33}^{S}\log(R_3/R_2)}, \tag{21}$$

$$\mathcal{L}_{\mathrm{p}} = \frac{1}{2}\int_{R_1}^{R_2}\left[\rho_{\mathrm{p}}u_r^2 - \overline{c}_{11}^{E}\left[\left(u_{r,r} + \frac{u_r}{r}\right)^2 - 2\left(1-\sigma_{12}^{E}\right)u_{r,r}\frac{u_r}{r}\right] - 2\overline{e}_{31}\left(u_{r,r} + \frac{u_r}{r}\right)\frac{v_{\mathrm{p}}}{h}\right](2\pi r h)\mathrm{d}r + \frac{1}{2}C_{\mathrm{p}}v_{\mathrm{p}}^2, \tag{22}$$

$$\mathcal{L}_{\mathrm{s}} = \frac{1}{2}\int_{R_2}^{R_3}\left[\rho_{\mathrm{s}}u_{\mathrm{r}}^2 - \overline{c}_{33}^{D}\left[\left(u_{r,r} + \nu\frac{u_r}{r}\right)^2 - 2\left(\nu - \overline{\sigma}_{13}^{D}\right)u_{r,r}\frac{u_r}{r}\right] - 2\left(\overline{h}_{33}u_{r,r} + \overline{h}_{31}\frac{u_r}{r}\right)\frac{q_{\mathrm{s}}}{2\pi r h}\right](2\pi r h)\mathrm{d}r - \frac{1}{2}\frac{q_{\mathrm{s}}^2}{C_{\mathrm{s}}}. \tag{23}$$

### *E. Application of Hamilton's Principle*

According to [19], a general form of Hamilton's principle applied to a PT is

$$\int_{t_{\mathrm{i}}}^{t_{\mathrm{f}}}(\delta\mathcal{L} + \delta\mathcal{W}_{\mathrm{ext}})\mathrm{d}t = 0, \tag{24}$$

where $\delta\mathcal{L}$ and $\delta\mathcal{W}_{\mathrm{ext}}$ are the variations of the PT's Lagrangian and the work done by external sources and forces on the time interval [$t_{\mathrm{i}}$, $t_{\mathrm{f}}$], respectively. The latter is expressed as follows:

$$\delta\mathcal{W}_{\mathrm{ext}}(t) = i_{\mathrm{p}}(t)\delta\lambda_{\mathrm{p}}(t) + f_{\mathrm{R}}(t)\delta q_{\mathrm{s}}(t), \tag{25}$$

with $f_{\mathrm{R}}(t)$ symbolizing a damping force, due to the Joule's first law in the load resistance, expressed by [20, ch. 3, sec. 3.4.3, p. 74, eq. 3.47],

$$f_{\mathrm{R}}(t) = -\frac{\partial R(\dot{q}_{\mathrm{s}}, t)}{\partial\dot{q}_{\mathrm{s}}}, \tag{26}$$

where $R(\dot{q}_{\mathrm{s}}, t)$, named the Rayleigh dissipation function, is defined by [20, ch. 3, sec. 3.4.3, p. 74, eq. 3.49],

$$R(\dot{q}_{\mathrm{s}}, t) = \frac{1}{2}R_L\dot{q}_{\mathrm{s}}^2(t). \tag{27}$$

In the previous relationship, the load resistance $R_{\mathrm{L}}$ plays the role of a dissipation constant linked with the generalized velocity $\dot{q}_{\mathrm{s}}$. The system configuration is besides supposed to be known at initial and final times, so that

$$\begin{aligned} \forall r \in [R_1, R_3],\, \delta u_r(r, t_{\mathrm{i}}) = \delta u_r(r, t_{\mathrm{f}}) &= 0 \\ \delta\lambda_{\mathrm{p}}(t_{\mathrm{i}}) = \delta\lambda_{\mathrm{p}}(t_{\mathrm{f}}) &= 0 \\ \delta q_{\mathrm{s}}(t_{\mathrm{i}}) = \delta\boldsymbol{q}_{\mathrm{s}}(t_{\mathrm{f}}) &= 0. \end{aligned} \tag{28}$$

On this basis, by means of integrations by parts on the spatial $r$ and time $t$ variables, the stationary of the definite

integral (24) leads to the equations governing the system dynamic. As a consequence, the equation of motion is expressed for both primary and secondary parts, as follows:

$$\begin{cases} \bar{c}_{11}^{E}\mathbb{B}_1[u_r(r,t)] = \rho_{\mathrm{p}}\ddot{u}_r(r,t), & r \in [R_1, R_2] \\ \bar{c}_{33}^{D}\mathbb{B}_\nu[u_r(r,t)] = \rho_{\mathrm{s}}\ddot{u}_r(r,t) + \bar{h}_{31}\dfrac{q_{\mathrm{s}}(t)}{2\pi r^2 h}, & r \in [R_2, R_3], \end{cases} \tag{29}$$

where $\mathbb{B}_\alpha[f]$ is an operator defined for $\alpha \in \mathbb{R}$ by

$$\mathbb{B}_\alpha[f] = f_{,rr} + \frac{1}{r}f_{,r} - \frac{\alpha^2}{r^2}f. \tag{30}$$

As well as the mechanical equation (29), two extra equations, respectively named actuator and sensor equations, are deduced from Hamilton's principle and take the following form:

$$i_{\mathrm{p}}(t) = C_{\mathrm{p}}\dot{v}_{\mathrm{p}}(t) - 2\pi\bar{e}_{31}[r\dot{u}_r(r,t)]_{R_1}^{R_2}, \tag{31}$$

$$\frac{q_{\mathrm{s}}(t)}{C_{\mathrm{s}}} = v_{\mathrm{s}}(t) - \int_{R_2}^{R_3}\left[\bar{h}_{33}u_{r,r}(r,t) + \frac{\bar{h}_{31}}{r}u_{\mathrm{r}}(r,t)\right]\mathrm{d}r. \tag{32}$$

Finally, in order that the problem may be well-defined, (29), (31), and (32) need to be completed with the boundary conditions (3) and (7) and the continuity relationships expressed at the junction between the driving and receiving sections as follows:

$$u_r(r = R_2^-, t) = u_r(r = R_2^+, t), \tag{33}$$

$$T_{rr}(r = R_2^-, t) = T_{rr}(r = R_2^+, t), \tag{34}$$

$$\phi(r = R_2^-, z, t) = \phi(r = R_2^+, z, t). \tag{35}$$

### *F. Problem Solving*

To solve the problem formulated in the previous section, following the standard modal expansion method, the radial displacement, solution of (29), can be written as an absolutely convergent series of the eigenfunctions as follows:

$$u_r(r,t) = \sum_{n=1}^{+\infty}\underline{u}_{r\infty}^{(n)}(r)\eta_n(t), \tag{36}$$

where $\underline{u}_{r\infty}^{(n)}(r)$ and $\eta_n(t)$ are respectively the mass normalized eigenfunction and the modal coordinate of the free-free PT with an open secondary part for the $n$th radial mode. Thereafter, the infinite subscript $(-\infty)$ will be used to remind this configuration.

*1) Determination of Eigenmodes:* The determination of eigenmodes is carried out for a free-free PT with a short-circuited primary part ($\forall t > 0, v_{\mathrm{p}}(t) = 0$) and an open secondary part ($\forall t > 0, q_{\mathrm{s}}(t) = 0$). Assuming that the mechanical and electrical quantities harmonically evolve, which means for the radial displacement that $u_{\mathrm{r}}(r,t) = \underline{u}_{r\infty}(r)\exp(j\omega t)$ with $j^2 = -1$ and $\underline{u}_{r\infty}(r)$ its amplitude at the angular frequency $\omega$, the mechanical equation (29) is reduced to

$$\begin{cases} \underline{u}_{r\infty,rr} + \dfrac{1}{r}\underline{u}_{r\infty,r} + \left[k_1^2 - \dfrac{1}{r^2}\right]\underline{u}_{r\infty} = 0, & r \in [R_1, R_2] \\ \underline{u}_{r\infty,rr} + \dfrac{1}{r}\underline{u}_{r\infty,r} + \left[k_2^2 - \dfrac{\nu^2}{r^2}\right]\underline{u}_{r\infty} = 0, & r \in [R_2, R_3], \end{cases} \tag{37}$$

where $k_1$ and $k_2$ are, respectively, the wave vectors within the primary and secondary parts whose expressions are

$$k_1 = \omega\sqrt{\frac{\rho_{\mathrm{p}}}{\bar{c}_{11}^{E}}} = \omega\sqrt{\rho_{\mathrm{p}}s_{11}^{E}\left[1 - (\sigma_{12}^{E})^2\right]}, \tag{38}$$

$$k_2 = \omega\sqrt{\frac{\rho_{\mathrm{s}}}{\bar{c}_{33}^{D}}} = \omega\sqrt{\rho_{\mathrm{s}}s_{33}^{E}\delta/(1 - k_{31}^2)}; \tag{39}$$

$\underline{u}_{r\infty}$ is thus the solution of a classical homogeneous Bessel's equation of order 1 and $v$ on the primary and secondary parts, respectively, so much that

$$\underline{u}_{r\infty}(r) = \begin{cases} A_u J_1(k_1 r) + B_u Y_1(k_1 r), & r \in [R_1, R_2] \\ C_u J_\nu(k_2 r) + D_u Y_\nu(k_2 r), & r \in [R_2, R_3], \end{cases} \tag{40}$$

where ($J_1$, $J_\nu$) and ($Y_1$, $Y_\nu$) are Bessel functions of the first and second kinds of orders 1 and $\nu$, respectively. $A_u$, $B_u$, $C_u$, and $D_u$ are constants of integration. Then, the expression of the electric potential can be obtained by injecting the part of (40) relative to the receiving section into the third equation of the constitutive relationship (9) and then integrating. Knowing that the primary part is short circuited, the electric potential $\underline{\phi}_{\infty}$ associated to the modal radial displacement $\underline{u}_{r\infty}$ is only nonzero on the receiving section with the following expression:

$$\underline{\phi}_{\infty}(r) = \bar{h}_{33}[C_u J_{-1,\nu}^{(h)}(k_2 r) + D_u Y_{-1,\nu}^{(h)}(k_2 r)] + D_\phi, \tag{41}$$

where the function $\mathcal{C}_{\mu,\nu}^{(h)}$, defined by (42), and the identity (43) [21, ch. X, sec. 10.74, p. 350, eq. 5] have been used with $\mathcal{C}$ being able to be equally substituted by $J$ or $Y$ in both relationships.

$$\forall z \in \mathbb{R}, \mathcal{C}_{\mu,\nu}^{(h)}(z) = \mathcal{C}_\nu(z) + \frac{\bar{h}_{31}}{\bar{h}_{33}}\int z^\mu \mathcal{C}_\nu(z)\mathrm{d}z. \tag{42}$$

It has to be noted that $s_{\mu,v}(z)$ symbolizes in the expression (43) the Lommel function of the first kind whose expression can be found in [21, ch. X, sec. 10.7, p. 346, eq. 10]. This function is a particular solution of a Lommel's differential equation (i.e., a nonhomogeneous Bessel's equation with a power function as the right-hand side):

$$\frac{[J_1^E(\xi_{11}^{(n)})Y_1^E(\xi_{12}^{(n)}) - J_1^E(\xi_{12}^{(n)})Y_1^E(\xi_{11}^{(n)})][J_\nu^D(\xi_{23}^{(n)})Y_\nu(\xi_{22}^{(n)}) - J_\nu(\xi_{22}^{(n)})Y_\nu^D(\xi_{23}^{(n)})]}{[J_1^E(\xi_{11}^{(n)})Y_1(\xi_{12}^{(n)}) - J_1(\xi_{12}^{(n)})Y_1^E(\xi_{11}^{(n)})][J_\nu^D(\xi_{23}^{(n)})Y_\nu^D(\xi_{22}^{(n)}) - J_\nu^D(\xi_{22}^{(n)})Y_\nu^D(\xi_{23}^{(n)})]} = \sqrt{\frac{\overline{c}_{33}^D}{\overline{c}_{11}^E}}, \tag{47}$$

$$\alpha_\infty^{(n)} = \sqrt{\frac{\overline{c}_{11}^E}{\overline{c}_{33}^D}}\frac{J_1^E(\xi_{11}^{(n)})Y_1^E(\xi_{12}^{(n)}) - J_1^E(\xi_{12}^{(n)})Y_1^E(\xi_{11}^{(n)})}{J_\nu^D(\xi_{23}^{(n)})Y_\nu^D(\xi_{22}^{(n)}) - J_\nu^D(\xi_{22}^{(n)})Y_\nu^D(\xi_{23}^{(n)})}, \tag{48}$$

$$\underline{u}_{r\infty}^{(n)}(r) = U_\infty^{(n)}\begin{cases} Y_1^E(\xi_{11}^{(n)})J_1(k_{1\infty}^{(n)}r) - J_1^E(\xi_{11}^{(n)})Y_1(k_{1\infty}^{(n)}r), & r \in [R_1, R_2] \\ \alpha_\infty^{(n)}[Y_\nu^D(\xi_{23}^{(n)})J_\nu(k_{2\infty}^{(n)}r) - J_\nu^D(\xi_{23}^{(n)})Y_\nu(k_{2\infty}^{(n)}r)], & r \in [R_2, R_3] \end{cases}, \tag{49}$$

$$\underline{\phi}_\infty^{(n)}(r) = \Phi_\infty^{(n)}\begin{cases} 0, & r \in [R_1, R_2] \\ \alpha_\infty^{(n)}[Y_\nu^D(\xi_{23}^{(n)})[J_{-1,\nu}^{(h)}(k_{2\infty}^{(n)}r) - J_{-1,\nu}^{(h)}(\xi_{22}^{(n)})] - J_\nu^D(\xi_{23}^{(n)})[Y_{-1,\nu}^{(h)}(k_{2\infty}^{(n)}r) - Y_{-1,\nu}^{(h)}(\xi_{22}^{(n)})]], & r \in [R_2, R_3]. \end{cases} \tag{50}$$

$\forall z \in \mathbb{R}, \mu \pm \nu \notin \{-2n-1; n \in \mathbb{N}\}$,

$$\int z^\mu \mathcal{C}_\nu(z)\mathrm{d}z = z[(\mu+\nu-1)\mathcal{C}_\nu(z)s_{\mu-1,\nu-1}(z) - \mathcal{C}_{\nu-1}(z)s_{\mu,\nu}(z)]. \tag{43}$$

In fact, it remains to determine five constants of integration ($A_u$, $B_u$, $C_u$, $D_u$, $D_\phi$) and the resonant angular frequency $\omega$ of the considered structure. To solve this problem, the boundary conditions (3) and the continuity relationships (33) to (35) have been used. The radial component of the stress tensor $\underline{T}_{rr}$ is deduced from the expression (40) inserted into the first equations of the constitutive relationships (8) and (9) so that

$$\underline{T}_{rr}(r) = \begin{cases} \overline{c}_{11}^E k_1[A_u J_1^E(k_1 r) + B_u Y_1^E(k_1 r)], & r \in [R_1, R_2] \\ \overline{c}_{33}^D k_2[C_u J_\nu^D(k_2 r) + D_u Y_\nu^D(k_2 r)], & r \in [R_2, R_3], \end{cases} \tag{44}$$

The Bessel's functions in (44) can be expressed by the generic forms $\mathcal{C}_1^E$ and $\mathcal{C}_\nu^D$ ($\mathcal{C}$ being able to be equally substituted by $J$ or $Y$) as follows:

$$\begin{aligned} \mathcal{C}_1^E(\xi) &= \mathcal{C}_0(\xi) - \frac{1-\sigma_{12}^E}{\xi}\mathcal{C}_1(\xi) \\ \mathcal{C}_\nu^D(\xi) &= \mathcal{C}_{\nu-1}(\xi) - \frac{\nu-\overline{\sigma}_{13}^D}{\xi}\mathcal{C}_\nu(\xi). \end{aligned} \tag{45}$$

Combining (40), (41), and (44) with the relationships (3) and (33) to (35), the following singular system is obtained:

$$\mathcal{M}_\infty(\omega)\begin{bmatrix} A_u \\ B_u \\ C_u \\ D_u \\ D_\phi \end{bmatrix} = \begin{bmatrix} 0 \\ 0 \\ 0 \\ 0 \\ 0 \end{bmatrix}, \tag{46}$$

where $\mathcal{M}_\infty(\omega)$ is a $5 \times 5$ matrix function of $\omega$. The resonant angular frequency $\omega_\infty^{(n)}$ is the $n$th root of the secular equation $\det[\mathcal{M}_\infty(\omega)] = 0$, which is explicitly given by (47) where $\xi_{ij}^{(n)} = k_{i\infty}^{(n)}R_j$ for $(i,j) \in 1;2\times 1;3$. The $n$th mechanical mode shape $\underline{u}_{r\infty}^{(n)}(r)$ and electric potential $\underline{\phi}_\infty^{(n)}(r)$ are defined, for instance, by expressing ($B_u$, $C_u$, $D_u$, $D_\phi$) as a function of the remaining constant of integration $A_u$ using (46) removed one line. The general solution of the proposed eigenvalue problem consequently takes the form given by the equations (49) and (50) where $U_\infty^{(n)} = A_\mathrm{u}/\,Y_1^E(\xi_{11}^{(n)})$, $\Phi_\infty^{(n)} = \overline{h}_{33}U_\infty^{(n)}$, and $\alpha_\infty^{(n)}$ is defined by (47), (48), (49), and (50), see above.

*2) Orthogonality of Eigenmodes:* Knowing that the $n$th mode shape verifies the spatial equation expressed on both primary and secondary parts as follows:

$$\begin{cases} \overline{c}_{11}^E\mathbb{B}_1[\underline{u}_\infty^{(n)}(r)] + \rho_\mathrm{p}[\omega_\infty^{(n)}]^2\underline{u}_{r\infty}^{(n)}(r) = 0, & r \in [R_1, R_2] \\ \overline{c}_{33}^D\mathbb{B}_\nu[\underline{u}_{r\infty}^{(n)}(r)] + \rho_\mathrm{s}[\omega_\infty^{(n)}]^2\underline{u}_{r\infty}^{(n)}(r) = 0, & r \in [R_2, R_3], \end{cases} \tag{51}$$

the multiplication of the previous equation by the $m$th mode shape $\underline{u}_{r\infty}^{(m)}(r)$ and an integration over the domain gives the relationship (52),

$$\begin{aligned} [\omega_\infty^{(n)}]^2 M^{(n,m)} &+ \int_{R_1}^{R_2}\underline{u}_{r\infty}^{(m)}(r)\overline{c}_{11}^E\mathbb{B}_1[\underline{u}_{r\infty}^{(n)}(r)](2\pi r h)\mathrm{d}r \\ &+ \int_{R_2}^{R_3}\underline{u}_{r\infty}^{(m)}(r)\overline{c}_{33}^D\mathbb{B}_\nu[\underline{u}_{r\infty}^{(n)}(r)](2\pi r h)\mathrm{d}r = 0. \end{aligned} \tag{52}$$

where $M^{(n,m)} = M_\mathrm{p}^{(n,m)} + M_\mathrm{s}^{(n,m)}$ with $M_\mathrm{p}^{(n,m)}$ and $M_\mathrm{s}^{(n,m)}$ the modal masses of the primary and secondary parts for the $n$th mode shape projected on the $m$th one, respectively, whose expressions are

$$M_{\mathrm{p}}^{(n,m)} = \int_{R_1}^{R_2} \underline{u}_{r\infty}^{(m)}(r)\rho_{\mathrm{p}}\underline{u}_{r\infty}^{(n)}(r)(2\pi rh)\mathrm{d}r, \tag{53}$$

$$M_{\mathrm{s}}^{(n,m)} = \int_{R_2}^{R_3} \underline{u}_{r\infty}^{(m)}(r)\rho_{\mathrm{s}}\underline{u}_{r\infty}^{(n)}(r)(2\pi rh)\mathrm{d}r. \tag{54}$$

Furthermore, the second part of the expression (52) can be rewritten by considering on the appropriate interval the following identities:

$$\left.\begin{matrix}\overline{c}_{11}^{E}\mathbb{B}_1[\underline{u}_{r\infty}^{(n)}(r)] \\ \overline{c}_{33}^{D}\mathbb{B}_\nu[\underline{u}_{r\infty}^{(n)}(r)]\end{matrix}\right\} = \underline{T}_{rr,r}^{(n)}(r) + \frac{1}{r}[\underline{T}_{rr}^{(n)}(r) - \underline{T}_{\theta\theta}^{(n)}(r)]. \tag{55}$$

As a consequence, an integration by parts on the space variable $r$ and the use of the boundary conditions (3) and the continuity relationship (34) lead to a simplification of (52) so much that

$$[\omega_\infty^{(n)}]^2 M^{(n,m)} - K^{(n,m)} = 0, \tag{56}$$

where $K^{(n,m)} = K_{\mathrm{p}}^{(n,m)} + K_{\mathrm{s}}^{(n,m)}$ with $K_{\mathrm{p}}^{(n,m)}$ and $K_{\mathrm{s}}^{(n,m)}$ the modal stiffnesses of the primary and secondary parts for the $n$th mode projected on the $m$th one, respectively. Their expressions are specified by the relationships (57) and (58). To show the orthogonality condition, the same procedure can be applied for the $m$th mode leading to

$$K_{\mathrm{p}}^{(n,m)} = \int_{R_1}^{R_2} \overline{c}_{11}^{E}\left[\left[\underline{u}_{r\infty,r}^{(m)}(r) + \frac{\sigma_{12}^{E}}{r}\underline{u}_{r\infty}^{(m)}(r)\right]\left[\underline{u}_{r\infty,r}^{(n)}(r) + \frac{\sigma_{12}^{E}}{r}\underline{u}_{r\infty}^{(n)}(r)\right] + \frac{1-(\sigma_{12}^{E})^2}{r^2}\underline{u}_{r\infty}^{(m)}(r)\underline{u}_{r\infty}^{(n)}(r)\right](2\pi rh)\mathrm{d}r, \tag{57}$$

$$K_{\mathrm{s}}^{(n,m)} = \int_{R_2}^{R_3} \overline{c}_{33}^{D}\left[\left[\underline{u}_{r\infty,r}^{(m)}(r) + \frac{\overline{\sigma}_{13}^{D}}{r}\underline{u}_{r\infty}^{(m)}(r)\right]\left[\underline{u}_{r\infty,r}^{(n)}(r) + \frac{\overline{\sigma}_{13}^{D}}{r}\underline{u}_{r\infty}^{(n)}(r)\right] + \frac{\nu^2 - \left(\overline{\sigma}_{13}^{D}\right)^2}{r^2}\underline{u}_{r\infty}^{(m)}(r)\underline{u}_{r\infty}^{(n)}(r)\right](2\pi rh)\mathrm{d}r, \tag{58}$$

$$[\omega_\infty^{(m)}]^2 M^{(m,n)} - K^{(m,n)} = 0. \tag{59}$$

Finally, by subtracting (59) from (56) and recalling that $m$ and $n$ are distinct modes ($\omega_\infty^{(m)} \neq \omega_\infty^{(n)}$), the symmetry of the modal mass and stiffness matrices [see the expressions (53) and (54), then (57) and (58)] enables to highlight the orthogonality condition of the eigenfunctions so much that

$$\forall (m,n) \in (\mathbb{N}^*)^2, \begin{cases} M^{(m,n)} &= \delta_{nm} \\ K^{(m,n)} &= \delta_{nm}\left[\omega_\infty^{(m)}\right]^2, \end{cases} \tag{60}$$

where $\delta_{nm}$ is the Kronecker's delta. By assuming that the PT is composed of the same material for the driving and receiving sections, which means $\rho_{\mathrm{p}} = \rho_{\mathrm{s}} = \rho$, the mode shapes can be normalized according to the modal mass normalization criterion (60) defined for this cylindrical structure by

$$\forall n \in \mathbb{N}^*, \int_{R_1}^{R_3} \rho[\underline{u}_{r\infty}^{(n)}(r)]^2(2\pi rh)\mathrm{d}r = 1. \tag{61}$$

It enables determination of the constant $U_\infty^{(n)}$ given by (64) where the expression (40) giving the modal radial displacement, to simplify the calculus, has been rewritten as follows:

$$\underline{u}_{r\infty}^{(n)}(r) = U_\infty^{(n)}\begin{cases}\mathcal{C}_{1,1}(r), & r \in [R_1, R_2] \\ \mathcal{C}_{2,\nu}(r), & r \in [R_2, R_3],\end{cases} \tag{62}$$

with $\mathcal{C}_{\alpha,\beta}(r)$ defined by

$$\mathcal{C}_{\alpha,\beta}(r) = A_\alpha J_\beta(k_{\alpha\infty}^{(n)}r) + B_\alpha Y_\beta(k_{\alpha\infty}^{(n)}r), \tag{63}$$

and by identification $A_1 = Y_1^E(\xi_{11}^{(n)})$, $B_1 = -J_1^E(\xi_{11}^{(n)})$, $A_2 = \alpha_\infty^{(n)}Y_\nu^D(\xi_{23}^{(n)})$, and $B_2 = -\alpha_\infty^{(n)}J_\nu^D(\xi_{23}^{(n)})$.

$$U_\infty^{(n)} = \Big[\rho\pi h([r^2[\mathcal{C}_{1,1}^2(r) - \mathcal{C}_{1,0}(r)\mathcal{C}_{1,2}(r)]]_{R_1}^{R_2} + [r^2[\mathcal{C}_{2,\nu}^2(r) - \mathcal{C}_{2,\nu-1}(r)\mathcal{C}_{2,\nu+1}(r)]]_{R_2}^{R_3})\Big]^{-1/2}. \tag{64}$$

*3) Response to a Harmonic Supply Voltage:* In this section, the PT is supposed to be supplied by a harmonic input voltage $v_p(t) = V_p\cos(\omega t)$. The solution of the mechanical equation (29) to this excitation can be expressed by means of (36) and the orthogonality condition (60) relative to the chosen eigenfunctions. To perform this, both equations of the equation of motion (29) are multiplied by the mass-normalized mode shape $\underline{u}_{r\infty}^{(m)}(r)$ and integrated over the primary and secondary sides, respectively. The result is shown by (65):

$$\sum_{n=1}^{+\infty}\Big\{M^{(n,m)}\ddot{\eta}_n(t) - \Big[\int_{R_1}^{R_2}\underline{u}_{r\infty}^{(m)}(r)\overline{c}_{11}^{E}\mathbb{B}_1[\underline{u}_{r\infty}^{(n)}(r)](2\pi rh)\mathrm{d}r + \int_{R_2}^{R_3}\underline{u}_{r\infty}^{(m)}(r)\overline{c}_{33}^{D}\mathbb{B}_\nu[\underline{u}_{r\infty}^{(n)}(r)](2\pi rh)\mathrm{d}r\Big]\eta_n(t)\Big\} = -q_s(t)\int_{R_2}^{R_3}\frac{\overline{h}_{31}}{r}\underline{u}_{r\infty}^{(m)}(r)\mathrm{d}r. \tag{65}$$

Then, by using the identity (55) and an integration by parts on the space variable $r$, the $\eta_n(t)$-coefficient in (65) can be simplified by the following quantity:

$$-K^{(n,m)} + [r\underline{u}_{r\infty}^{(m)}(r)\underline{T}_{rr}^{(n)}(r)]_{R_1}^{R_3}. \tag{66}$$

Finally, by invoking the orthogonality condition (60) and using the boundary conditions (3) and the continuity of the radial stress (34), it results an infinite system of mechanical equations as follows:

$$\forall n \in \mathbb{N}^*, \ddot{\eta}_n(t) + [\omega_\infty^{(n)}]^2\eta_n(t) = \psi_{p\infty}^{(n)}v_p(t) - \chi_{s\infty}^{(n)}q_s(t), \tag{67}$$

$$\forall n \in \mathbb{N}^*, \ddot{\eta}_n(t) + \frac{\omega_\infty^{(n)}}{Q_m^{(n)}}\dot{\eta}_n(t) + [\omega_\infty^{(n)}]^2\eta_n(t) - \chi_{s\infty}^{(n)}\sum_{r=1}^{+\infty}\psi_{s\infty}^{(r)}\eta_r(t) = \psi_{p\infty}^{(n)}v_p(t) - \psi_{s\infty}^{(n)}v_s(t) \text{ (mechanical eq.)},$$
$$i_p(t) = C_p\dot{v}_p(t) + \sum_{r=1}^{+\infty}\psi_{p\infty}^{(r)}\dot{\eta}_r(t) \text{ (actuator eq.)}, \tag{70}$$
$$\sum_{r=1}^{+\infty}\psi_{s\infty}^{(r)}\dot{\eta}_r(t) = C_s\dot{v}_s(t) + i_s(t) \text{ (sensor eq.)},$$

where $\psi_{p\infty}^{(n)}$ and $\chi_{s\infty}^{(n)}$ are the electromechanical coupling factors within the primary and secondary sides for the $n$th mode shape.

$$\forall n \in \mathbb{N}^*, \psi_{p\infty}^{(n)} = -2\pi\bar{e}_{31}U_\infty^{(n)}[R_2\mathcal{C}_{1,1}(R_2) - R_1\mathcal{C}_{1,1}(R_1)], \tag{68}$$

$$\forall n \in \mathbb{N}^*, \chi_{s\infty}^{(n)} = U_\infty^{(n)}\big[\bar{h}_{33}\mathcal{C}_{2,\nu}(\xi) + \bar{h}_{31}\xi[(\nu-2)\mathcal{C}_{2,\nu}(\xi)s_{-2,\nu-1}(\xi) - \mathcal{C}_{2,\nu-1}(\xi)s_{-1,\nu}(\xi)]\big]_{\xi_{22}^{(n)}}^{\xi_{23}^{(n)}}. \tag{69}$$

The previous equation can be expressed in function of the secondary voltage $v_s(t)$ by using the sensor equation (32) so much that the equations governing the electrodynamical behavior of the PT are obtained and can be summarized in (70), see above, where the relationship $\psi_{s\infty}^{(n)} = C_s\chi_{s\infty}^{(n)}$ has been used. Moreover, a modal mechanical quality factor $Q_m^{(n)}$ has been added in the mechanical equation in (70), which will be able to be experimentally deduced or arbitrarily set. It has to be noticed that the radial modes are coupled by crossed terms that can be interpreted as an extra stiffness in the mechanical equation. The system of (70) is uncoupled for an open circuit condition ($q_s = 0$), in accordance with the chosen modal basis, in such a way that for $n \in \mathbb{N}^*$:

$$\begin{cases} \ddot{\eta}_n(t) + \dfrac{\omega_\infty^{(n)}}{Q_m^{(n)}}\dot{\eta}_n(t) + \left[\omega_\infty^{(n)}\right]^2\eta_n(t) = \psi_{p\infty}^{(n)}v_p(t), \\ i_p(t) = C_p\dot{v}_p(t) + \displaystyle\sum_{r=1}^{+\infty}\psi_{p\infty}^{(r)}\dot{\eta}_r(t), \\ \displaystyle\sum_{r=1}^{+\infty}\psi_{s\infty}^{(r)}\eta_r(t) = C_sv_s(t). \end{cases} \tag{71}$$

It is possible to give the expression of the input admittance $\underline{Y}_{p\infty} = \underline{i}_p/\underline{v}_p$ from the actuator and the mechanical equations in (71) so much that

$$\underline{Y}_{p\infty}(\omega) = j\omega\left[C_p + \sum_{n=1}^{+\infty}\frac{C_{m\infty}^{(n)}}{1 - X^2 + jX/Q_m^{(n)}}\right], \tag{72}$$

where $X = \omega/\omega_\infty^{(n)}$ is a dimensionless angular frequency and $C_{m\infty}^{(n)} = \left[\psi_{p\infty}^{(n)}/\omega_\infty^{(n)}\right]^2$ is the motional capacitance of the $n$th radial mode. Thereafter, putting this method into practice will need to truncate the modal basis to a few modes, for instance $N$. The required quantities to obtain this model are consequently:

- the first $N$ resonant angular frequencies $(\omega_\infty^{(n)})_{n\in1,N}$, mode shapes $(\underline{u}_{r\infty}^{(n)})_{n\in1,N}$ and mechanical quality factors $(Q_m^{(n)})_{n\in1,N}$ for an open ring Rosen-type PT,
- the first $N$ electromechanical coupling factors $(\psi_{p\infty}^{(n)})_{n\in1,N}$ and $(\chi_{s\infty}^{(n)})_{n\in1,N}$ of the primary and secondary parts,
- the input and output clamped capacitances $C_p$ and $C_s$.

## III. Numerical and Experimental Validation

To validate the relevance of the previously developed analytical modeling, numerical simulations and experimental characterizations were carried out. The numerical study takes advantage of a finite element method using the ANSYS software. A 2-D study assuming plane stress motion has effectively enabled to plot the mechanical mode shapes and the distribution of the electric potential along a radius of the considered structure. Regarding the experimental validation, this one is based on admittance measurements with an impedance analyzer (Agilent Technologies, HP4294A). This validation has been undertaken on four samples, named (S1) to (S4), composed of the PZT-type material APC841. All the PTs have the same dimensions, their differentiation only relying on a different intermediate radius, $R_2$ from 10 mm (S1) to 13 mm (S4). The geometrical and structural parameters of these PTs are itemized in Table III, where $\varepsilon_0 = 8.854 \times 10^{-12}$ symbolizes the vacuum permittivity.

First of all, the Table IV allows to compare the resonant frequencies of a ring Rosen-type PT with an open secondary part for the first three radial modes and for the four considered samples. The results from the analytical modeling, the numerical simulation and experimental measurements are very satisfactory, as confirmed by the percent error between the theoretical and experimental values (see Error [%] in Table IV). However, it has to be noticed that this error increases with the mode rank. It is due to the initial assumptions, essentially M1, M2, and M3.

TABLE III. Material Properties of APC841 Ceramic and Geometric Parameters of Ring Rosen-Type PTs.

| | Definition | Value | Unity |
|---|---|---|---|
| $R_1$ | Inner radius | 4 | mm |
| $R_2$ | Intermediate radius | [10, 13] | mm |
| $R_3$ | Outer radius | 20 | mm |
| $h$ | Thickness | 1 | mm |
| $\rho$ | Mass density | 7652 | kg/m$^3$ |
| $s_{11}^E$ | Transversal compliance at constant **E** | 11.7 | $\mu$m$^2$/N |
| $s_{12}^E$ | Transversal compliance at constant **E** | $-6.3$ | $\mu$m$^2$/N |
| $s_{13}^E$ | Transversal compliance at constant **E** | $-4.2$ | $\mu$m$^2$/N |
| $s_{33}^E$ | Longitudinal compliance at constant **E** | 13.9 | $\mu$m$^2$/N |
| $d_{31}$ | Transversal piezoelectric coefficient | $-100$ | pm/V |
| $d_{33}$ | Longitudinal piezoelectric coefficient | 280 | pm/V |
| $\varepsilon_{33}^T$ | Longitudinal permittivity at constant **T** | 1380 $\varepsilon_0$ | F/m |
| $k_{31}$ | Transversal coupling factor | 0.264 | |
| $k_{33}$ | Longitudinal coupling factor | 0.679 | |
| $Q_{\mathrm{m}}$ | Mechanical quality factor | 1300 | |

Additionally, the measurements of the input admittance and its theoretical evaluation by the expression (72) are presented on a wide frequency range. For readability reasons, only experimental and theoretical results of samples (S1) and (S4) are presented, in Figs. 2(a) and 2(b), respectively. Amplitude and phase are plotted on the same graph for qualitative comparison between modeling and measurements. The computation of the formula (72) has been performed for the first $N = 100$ radial modes. The modal mechanical quality factors $Q_{\mathrm{m}}^{(n)}$ have been identified with their experimental values for the first three modes and set to the material value for the remaining modal quantities. The accuracy is quite satisfying with an error increasing with the mode rank, even with a greater number $N$ of radial mode shapes considered for the computation. It is a typical limitation of the initial assumptions when mechanical wavelength is reduced. It tends to demonstrate that the range of interest for this modeling is limited to the rank of first modes. Another origin of discrepancy between theory and experiment may be the polarization process which does not necessarily ensure a perfect radially polarized secondary part. Indeed, to polarize the receiving part, a constant potential difference is applied between the intermediate radius $R_2$ and the outer radius $R_3$. As a consequence, because of the cylindrical geometry, a spatially variable electric field ($\propto 1/r$) is induced.

Despite this observed disparity, the theoretical approach enables to thoroughly study the influence of the geometric parameters in view of a PT's design dedicated to a specific application. For instance, within the framework of the plasma generation obtained by piezoelectric sources (see [22] for more details), it is obvious that the electric potential and its distribution are essential criteria for the promotion of ac plasma discharges. Indeed, the plasma discharge is strongly dependent on the electric field in the gas surrounding the transformer. The voltage value obtained on the surface and more particularly at the edge of the ring can be the local origin of the ignition and the sustainability of the discharge. It is consequently function of the radial mode.

Fig. 3 shows the normalized electric potential distribution on the ring surface along the radius for the first four radial modes. Parametric influence of the intermediate radius $R_2$ is also illustrated in accordance with existing samples (S1) to (S4). It has to be noted that the developed model also gives the opportunity to draw the normalized radial displacement from (40). Although the curves in Fig. 3 do not inform about the absolute voltage value (normalized curves), it is possible to discuss the different modes.

Among the four modes, the second and the fourth are particularly interesting. The former reaches the maximum voltage at the edge of the ring. Thus, the electric field in the gas immediately surrounding the edge could be very high. As a consequence, the plasma discharge may appear at the edge, all around the ring. Additionally, the fourth mode presents two optimum values, positive and negative. This configuration gives the opportunity to reach

TABLE IV. Resonant Frequencies of a Ring Rosen-Type PT With an Open Secondary Side for the First Three Radial Mode, Samples (S1) to (S4), Comparison of the Analytical (Anal.), Numerical (Num.), and Experimental (Exp.) Results.

| $f_\infty^{(n)}$ | Mode 1 | | | | Mode 2 | | | | Mode 3 | | | |
|---|---|---|---|---|---|---|---|---|---|---|---|---|
| [Hz] | Anal. | Num. | Exp. | Error [%] | Anal. | Num. | Exp. | Error [%] | Anal. | Num. | Exp. | Error [%] |
| (S1) | 53 056 | 53 115 | 51 794 | 2.4 | 147 077 | 145 628 | 144 737 | 1.6 | 265 324 | 262 029 | 250 192 | 5.7 |
| (S2) | 53 541 | 53 594 | 51 493 | 3.8 | 145 074 | 143 910 | 142 356 | 1.9 | 265 808 | 262 553 | 249 187 | 6.2 |
| (S3) | 53 998 | 54 048 | 51 445 | 4.7 | 143 442 | 142 545 | 141 649 | 1.2 | 266 026 | 262 820 | 250 527 | 5.8 |
| (S4) | 54 418 | 54 465 | 51 349 | 5.6 | 142 238 | 141 582 | 139 037 | 2.3 | 265 251 | 262 229 | 248 774 | 6.2 |

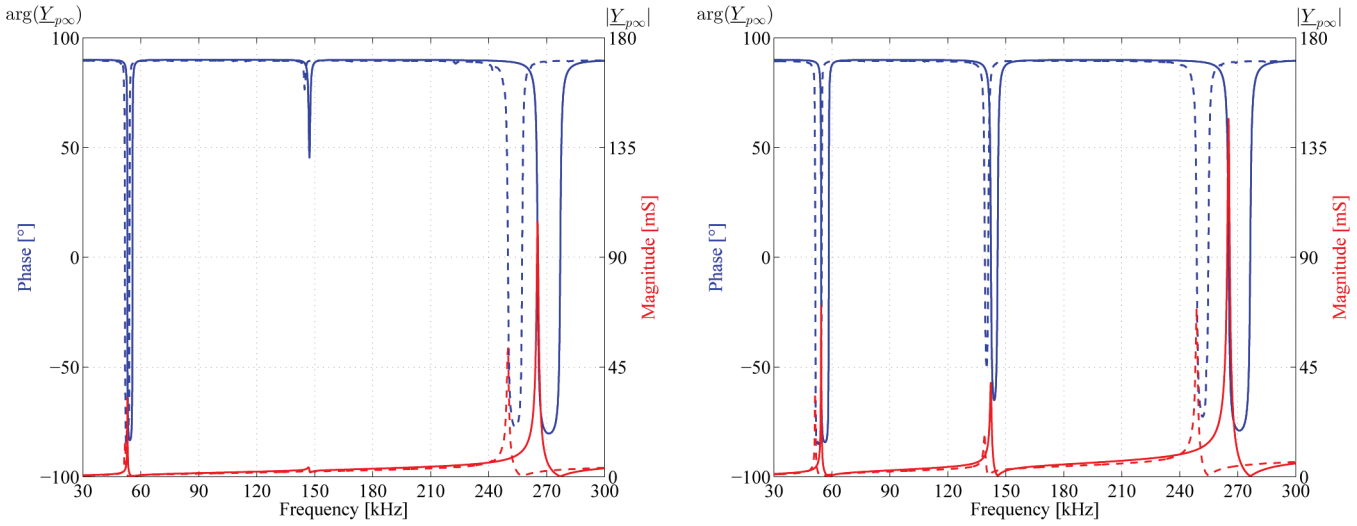


(a) Sample (S1)

(b) Sample (S4)

Fig. 2. Theoretical (solid line) and experimental (dashed line) input admittance (magnitude and phase) for samples (S1) and (S4).

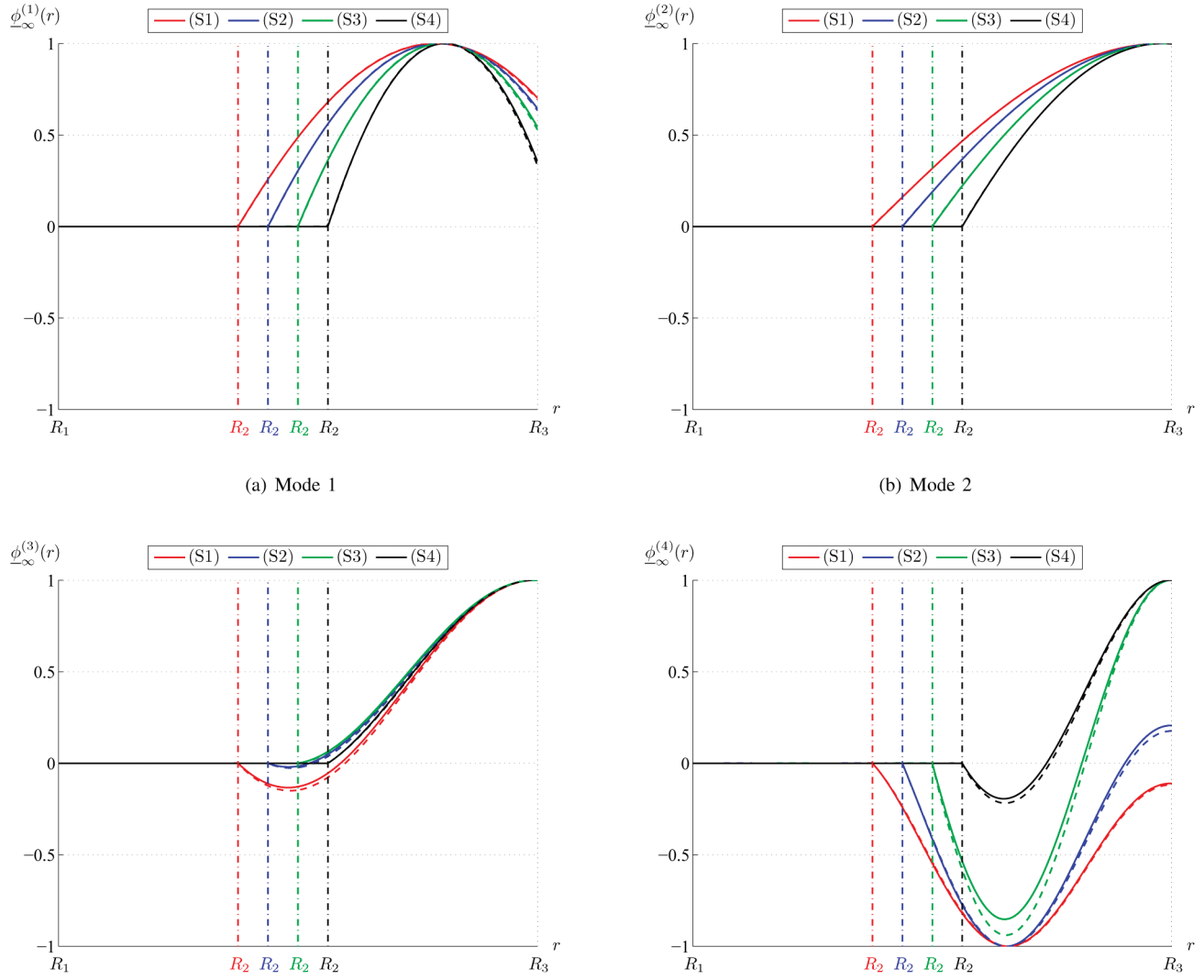


(a) Mode 1

(b) Mode 2

(c) Mode 3

(d) Mode 4

Fig. 3. Theoretical (solid line) and numerical (dashed line) electric potential of a ring Rosen-type PT: samples (S1) to (S4), first four radial modes.

very high electric field on the ring surface, especially in the illustrated configuration (S3). In such configuration, plasma discharge will appear on the ring surface, mainly located between $R_2$ and $R_3$. Other modes may also be useful to change the plasma patterns. As a consequence, by cautiously observing Fig. 3, it clearly appears that the intermediate radius and the radial mode shapes can be the subject of a future optimization in view of designing a PT dedicated to plasma generation with a voltage gain as high as possible. Moreover, it has to be noticed that operating frequency is an essential parameter for the piezoelectric device as well as for the plasma discharge behavior. Indeed, the step-up voltage is only efficient close to one of the resonance frequencies of the transformer. Likewise, the produced ac electric field may strongly affect the plasma discharges because of the dynamic behavior of the electric charges (sheath formation, ignition, extinction, etc.). As a consequence, specific attention will be paid to the optimization of the resonant frequency and the resulting design of the device.

## IV. Conclusion

This paper has demonstrated full analytical modeling for a ring Rosen-type PT. The application of Hamilton's principle has enabled establishment of the equations governing the electromechanical behavior of the considered structure. The problem has been solved with the classical modal expansion method, and the case of a PT with an open secondary has been more precisely studied and validated with numerical and experimental results. With the purpose of using this device as plasma discharge generator, one of the essential pieces of information is the electric potential distribution on the surface of the transformer. The results have shown that several vibratory modes are interesting to investigate and to be specifically the target of optimization to increase the electric field. This work has been the first step of an extended study that will include optimization of design, carrying out deterministic methods based on an analytical behavioral model [23], and plasma discharge characterizations.

## References


[1] C. A. Rosen, K. A. Fish, and H. C. Rothenberg, "Electromechanical transducer," U.S. Patent 2 830 274, Apr. 8, 1958.

[2] S. Manuspiya, T. Ezaki, B. Koc, and K. Uchino, "Laptop adaptor using a piezoelectric transformer—Drive circuit development," in *5th Int. Conf. on Intelligent Materials*, Penn State, PA, USA, Jun. 2003.

[3] M. Day and B. S. Lee, "Understanding piezoelectric transformers in CCFL backlight applications," *Analog Applications Journal*, Texas Instruments Incorporated, pp. 18–23, 2002.

[4] G. H. Hufferd, H. L. Vail, Jr., and R. H. Josephson, "Voltage or spark source," U.S. Patent 3 082 333, Mar. 19, 1963.

[5] S. H. Newman, "Cigarette lighter," U.S. Patent 3 295 024, Dec. 27, 1966.

[6] H. Itoh, K. Teranishi, and S. Suzuki, "Observation of light emissions around a piezoelectric transformer in various gases," *IEEE Trans. Plasma Sci.*, vol. 30, no. 1, pp. 124–125, Feb. 2002.

[7] K. Teranishi, D. Inada, N. Shimomura, S. Suzuki, and H. Itoh, "VUV spectroscopic measurement for dielectric barrier discharge excited by piezoelectric transformer in He-Xe mixture," *IEEE Trans. Plasma Sci.*, vol. 36, no. 4, pp. 1340–1341, Aug. 2008.

[8] M. Teschke and J. Engemann, "Low voltage APP-generation by piezo ceramics: Basic Structures, electro-mechanical simulations and poling techniques," in *Proc. 18th Int. Symp. Plasma Chemistry*, Kyoto, Japan, Aug. 26–31, 2007.

[9] H. Kim, A. Brockhaus, and J. Engemann, "Atmospheric pressure argon plasma jet using a cylindrical piezoelectric transformer," *Appl. Phys. Lett.*, vol. 95, issue 21, art. no. 211501, 2009.

[10] J. Engemann and M. Teschke, "Device for producing an atmospheric pressure plasma," U.S. Patent 2009/0122941 A1, May 14, 2009.

[11] J. S. Yang and X. Zhang, "Extensional vibration of a nonuniform piezoceramic rod and high voltage generation," *Int. J. Appl. Electromagn. Mechan.*, vol. 16, no. 1–2, pp. 29–42, Jan. 2002.

[12] C. Nadal and F. Pigache, "Multimodal electromechanical model of piezoelectric transformers by Hamilton's principle," *IEEE Trans. Ultrason. Ferroelectr. Freq. Control*, vol. 56, no. 11, pp. 2530–2543, Nov. 2009.

[13] J. S. Yang and X. Zhang, "Analysis of a thickness-shear piezoelectric transformer," *Int. J. Appl. Electromagn. Mechan.*, vol. 21, no. 2/2005, pp. 131–141, Apr. 2005.

[14] P. Půlpán and J. Erhart, "Transformation ratio of ring-dot planar piezoelectric transformer," *Sens. Actuators A*, vol. 140, no. 2, pp. 215–224, Nov. 2007.

[15] S. Lin, J. Hu, and Z. Fu, "Electromechanical characteristics of piezoelectric ceramic transformers in radial vibration composed of concentric piezoelectric ceramic disk and ring," *Smart Mater. Struct.*, vol. 22, no. 4, art. no. 045018, Mar. 2013.

[16] W. Chen, C. Lu, J. Yang, and J. Wang, "A circular cylindrical, radially polarized ceramic shell piezoelectric transformer," *IEEE Trans. Ultrason. Ferroelectr. Freq. Control*, vol. 56, no. 6, pp. 1238–1245, Jun. 2009.

[17] J. S. Yang, *An Introduction to the Theory of Piezoelectricity*. New York, NY, USA: Springer Science+Business Media Inc., 2005.

[18] T. Ikeda, *Fundamentals of Piezoelectricity*. New York, NY, USA: Oxford University Press Inc., 1996.

[19] C. Nadal, "Contribution to the conception and the modeling of piezoelectric transformers dedicated to plasma generation," Thèse de doctorat, Institut National Polytechnique de Toulouse, Toulouse, France, Jul. 2011 (in French).

[20] A. Preumont, *Mechatronics: Dynamics of Electromechanical and Piezoelectric Systems*. Dordrecht, The Netherlands: Springer-Verlag, 2006.

[21] G. N. Watson, *A Treatise on the Theory of Bessel Functions*, Seaside, OR, USA: Watchmaker Publishing, 2008.

[22] T. Martin, F. Pigache, C. Nadal, and T. Callegari, "Experimental analysis of piezoelectric plasma discharge generator," in *IEEE Int. Ultrasonics Symp.*, pp. 1–5, Dresden, Germany, Oct. 7–10, 2012.

[23] F. Pigache, F. Messine, and B. Nogarede, "Optimal design of piezoelectric transformers: A rational approach based on an analytical model and a deterministic global optimization," *IEEE Trans. Ultrason. Ferroelectr. Freq. Control*, vol. 54, no. 7, pp. 1293–1302, Jul. 2007.



**Clément Nadal** was born in Rennes, France, in 1983. He received an engineer's degree in electrical engineering and a M.S. degree in 2007 from École Nationale Supérieure d'Électrotechnique, d'Électronique, d'Informatique, d'Hydraulique et des Télécommunications (ENSEEIHT), Toulouse, France. He received a Ph.D. degree in electrical engineering from Institut National Polytechnique de Toulouse (INPT) in 2011, for his dissertation regarding analytical piezoelectric device modeling dedicated to plasma generation. He currently occupies a postdoctoral position at IRCICA (Institut de Recherche sur les Composants logiciels et matériels pour l'Information et la Communication Avancée), University of Lille 1, France, for the design of piezoelectric devices used for tactile applications.

**François Pigache** was born in Auchel, France, in 1977. He received a M.S. degree in instrumentation and advanced analysis in 2001, and a Ph.D. degree in electrical engineering from the University of Sciences and Technology, Lille, France, in 2005. He joined the Laboratoire des Plasmas et de la Conversion d'Énergie, Toulouse, France, as an associate professor. His research concerns multiphysic modeling, the optimization of piezoelectric transformers, and alternative applications of ferroelectric materials.

**Jiří Erhart** received his M.Sc. diploma from the Faculty of Mathematics and Physics, Charles University in Prague, Czech Republic, in the field of mathematical physics in 1988 and his Ph.D. in the field of condensed matter physics in 1999. He worked at the Institute of Physics, Academy of Sciences of the Czech Republic during 1990–1993. Currently he is working at the Technical University of Liberec, Czech Republic. He is head of Piezoelectricity Research Laboratory at the Department of Physics. He was promoted to associate professor in 2001 and to full professor in 2012. During 1998–1999 he worked as a research fellow and post-doc in the Materials Research Laboratory at The Pennsylvania State University, University Park, USA. In 2003 he was awarded The Matsumae International Foundation fellowship for his research stay at the Tokyo Institute of Technology, Japan. He also worked as a visiting research fellow at the City University in Hong Kong and at the Harbin Institute of Technology, China, for shorter stays during 2002, 2004, and 2009. Prof. Erhart specializes in the field of piezoelectricity and piezoelectric materials, ferroelectric domains and domain engineering, piezoelectric ceramics transformers, resonators, and actuators.